

Effect of high glucose on gene expression in mesangial cells: Up-regulation of the thiol pathway is an adaptational response

Jolean Morrison¹, Kristen Knoll¹, Martin J. Hessner^{2,3}, and Mingyu Liang¹

¹Departments of Physiology, and ²the Max McGee National Research Center for Juvenile Diabetes, Department of Pediatrics, Medical College of Wisconsin, Milwaukee, WI 53226; ³the Children's Research Institute of the Children's Hospital of Wisconsin, Milwaukee, WI 53226

Running head: High glucose, gene expression, and thiols in mesangial cells

Correspondence:

Mingyu Liang, M.B., Ph.D.
Department of Physiology
Medical College of Wisconsin
8701 Watertown Plank Road
Milwaukee, WI 53226
Tel: 414 456-8539
Fax: 414 456-6546
Email: mliang@mcw.edu

Abstract

Pathological alterations in glomerular mesangial cells play a critical role in the development of diabetic nephropathy, the leading cause of end-stage renal disease. Molecular mechanisms mediating such alterations, however, remain to be fully understood. The present study first examined the effect of high glucose on the mRNA expression profile in rat mesangial cells using cDNA microarray. Based on variation-weighted criteria and with a false discovery rate of 4.3%, 459 of 17,664 cDNA elements examined were found to be up-regulated and 151 down-regulated by exposure to 25 mM D-glucose for 5 days. A large number of differentially expressed genes belonged to several functional categories, indicating high glucose had a profound effect on mesangial cell proliferation, protein synthesis, energy metabolism, and, somewhat unexpectedly, protein sorting and the cytoskeleton. Interestingly, several thiol anti-oxidative genes (glutathione peroxidase 1, peroxiredoxin 6, and thioredoxin 2) were found by microarray and confirmed by real-time PCR to be up-regulated by high glucose. These changes suggested that the oxidative stress known to be induced in mesangial cells by high glucose might be buffered by up-regulation of the thiol anti-oxidative pathway. Up-regulation of thiol anti-oxidative genes also occurred in high glucose-treated human mesangial cells and in glomeruli isolated from rats after one week of streptozotocin-induced diabetes, but not in human proximal tubule cells. High glucose slightly increased lipid peroxidation and decreased the amount of reduced thiols in rat and human mesangial cells. Disruption of the thiol anti-oxidative pathway by two different thiol-oxidizing agents resulted in a 3-5 fold increase in high-glucose induced lipid peroxidation. In summary, the present study provided a global view of the short-term

effect of high glucose on mesangial cells at the level of mRNA expression and identified the up-regulation of the thiol anti-oxidative pathway as an adaptational response of mesangial cells to high glucose.

Key words: diabetes, diabetic nephropathy, microarray, oxidative stress, adaptation.

Diabetic nephropathy, a common complication of diabetes, is the leading cause of end-stage renal disease in the US (41). Diabetic nephropathy involves both glomerular and tubular-interstitial compartments. Abnormal extracellular matrix deposition, cellular growth, proliferation, and the impairment of function in glomerular mesangial cells contribute importantly to the progression of glomerular injury that eventually leads to glomerulosclerosis and renal failure in diabetic nephropathy (1, 33, 42).

While other abnormalities occurring in diabetes may participate in causing the pathological alterations of mesangial cells, hyperglycemia is believed to be the most important factor. High concentrations of glucose could damage mesangial cells through the stimulation of several interrelated pathways involving transforming growth factor- β , the polyol pathway, protein kinase C, the hexoamine pathway, or oxygen free radicals (3, 11). It is conceivable, however, that additional pathways or currently unrecognized aspects of the above pathways may also participate in mediating the effect of high glucose on mesangial cells. Identifying those new molecular elements and integrating fragmental molecular events into a cohesive global view are important for obtaining deeper insights into the mechanism of diabetic nephropathy and for discovering potential new therapeutic targets.

High-throughput gene expression profiling (27) is a powerful approach for obtaining global views of biological events and for generating novel hypotheses. A number of previous studies have attempted to assess the effect of high glucose on mesangial cell gene expression on a large scale using techniques such as mRNA differential display (17), suppression subtractive hybridization (5, 35), and Affymetrix GeneChip (22). Interesting changes of gene expression were identified in these studies,

demonstrating the discovery power of these high-throughput approaches. The present study extended this line of work by first producing an extensive gene expression profile of rat mesangial cells exposed to normal or high glucose. Taking advantage of recent advances in expression profiling and analytical techniques (27), the present study utilized a cDNA microarray containing ~18,000 elements, an experimental design incorporating several replicates, and a variation-weighted statistical method for identifying differential expression. Results of the expression profiling indicated a number of prominent global characteristics of the effect of high glucose on mesangial cells that had not been emphasized previously. Furthermore, a hypothesis that high glucose-induced oxidative injury in mesangial cells was buffered by up-regulation of the thiol anti-oxidative pathway was generated by this expression profiling and subsequently tested.

Materials and Methods

Materials. Chemicals and molecular grade solutions were obtained from Sigma (St. Louis, MO) and Invitrogen (Carlsbad, CA), respectively, unless otherwise indicated. Plastic supplies for cell culture were from Corning (Corning, NY) or Becton Dickinson (Franklin Lakes, NJ).

Cell culture. Immortalized rat mesangial cells obtained from American Type Culture Collection (Manassas, VA) were cultured in Dulbecco's Modified Eagle's Medium containing 5 mM D-glucose that was supplemented with 0.4 mg/ml G418 and 15% fetal bovine serum. Cells were propagated for at least 5 passages in this medium in the investigators' laboratory to verify stable growth characteristics and morphological features prior to treatment. Human mesangial cells and proximal tubule epithelial cells were obtained from Cambrex Bio Science (Walkersville, MD) and cultured in cell type-specific media supplied by the vendor of the cells. These media contained 5~7 mM D-glucose. Culture medium with additional D-glucose added to a final concentration of 25 mM was used for high glucose treatment. Culture medium with 20 mM D-mannitol or L-glucose added was used as normal glucose control. No apparent differences in the measurements performed in this study were observed between cells with D-mannitol or L-glucose supplementation. Culture medium was changed every two days during treatment. The D-glucose concentration in the high glucose culture medium after 2 days of incubation was above 18 mM as measured with a Glucometer (Roche Diagnostics, Basel, Switzerland).

Construction of cDNA microarrays. Rat cDNA microarrays were essentially constructed as described previously (12, 13). 18,432 elements were printed, including

768 controls (GAPDH, β -actin, arabidopsis clones, printing buffer, etc.) and 17,664 rat cDNA clones obtained from University of Iowa. cDNA clones were amplified, purified, quantified, and reconstituted at 150 ng/ μ l in 3% DMSO/1.5 M betaine for printing using a GeneMachines Omni Grid printer (San Carlos, CA). Printed arrays were post-processed using a non-aqueous method (9).

Microarray hybridization. RNA extraction, cDNA labeling, microarray hybridization and scanning, and raw data extraction were performed as described previously (30, 31). Briefly, 30 μ g of total RNA extracted from mesangial cells were reverse-transcribed to cDNA using oligo-(dT)₁₂₋₁₈ as the primer and labeled with fluorescent dyes Cy3 or Cy5. cDNAs derived from cells treated with normal and high glucose were labeled with different dyes, and pooled, purified, and hybridized together to a microarray. Hybridized microarrays were scanned and digitized using a confocal scanner. Raw values of fluorescent intensity in the signal and background areas of each spot were extracted using the software ImaGene 4.01 (BioDiscovery, Los Angeles, CA). The entire raw dataset has been deposited into Gene Expression Omnibus (<http://www.ncbi.nlm.nih.gov/geo>, series GSE1027).

Four separate cell preparations were examined for each treatment condition. cDNAs from cells treated with normal glucose were labeled with Cy3 and those from high glucose-treated cells were labeled with Cy5 in two microarrays, while the dyes were reversed in the other two microarrays. This design incorporated both biological replication and dye switching, and had been shown by a previous analysis to be robust yet cost-effective (26).

Microarray data analysis and annotation. Microarray data were processed as described previously (30, 31). Briefly, fluorescent intensity data were filtered and adjusted, and the ratio between high glucose and normal glucose calculated for each cDNA element on the array that passed the detectability and quality filters. Ratios were ln-transformed and normalized. 7,499 of 17,664 cDNA elements passed the detectability and quality filters consistently in all four microarrays.

A statistical method for identifying differentially expressed genes incorporating permutation and considerations of variance among biological samples has been described previously (40). The original version of the above method was designed for analyzing intensity data. The two-color hybridization method used in the present study allows analysis to be performed using ratios within array. To preserve this advantage, the statistical method mentioned above was slightly modified to analyze ln(ratio) data in the present study. Mean and s.d. of ln(ratio) were calculated for each of 7,499 cDNA elements that had passed the filters and yielded ln(ratio)s in all four arrays. A t value was calculated for each element as the absolute value of mean/s.d. The ln(ratio) data were rearranged to create balanced permutations that had an equal number of normal glucose and high glucose samples as well as an equal number of Cy3 and Cy5 in the numerators and the denominators. A t_p value was similarly calculated for each element in each permutation. An arbitrary value of t was set as the threshold of differential expression. cDNA elements that had t values (t_p in the case of permuted data sets) greater than the threshold t value were identified. False discovery rate was calculated as the average number of elements identified in permuted data sets divided by the number of elements

identified in the actual experimental data set. The threshold t value was then adjusted until the desired false discovery rate was achieved.

The original document for cDNA elements printed on the array contained the description, GenBank accession number, clone ID, Unigene cluster ID, and other information for each element. Additional annotation was performed for cDNA elements identified as differentially expressed. This included searching homologies for EST elements, identifying gene functions, and establishing pathway affiliation. Numerous publications and publicly available databases were utilized, examples of which included the NCBI databases (<http://www.ncbi.nih.gov>), the rat genome database (<http://rgd.mcw.edu>), and Swiss-Prot (<http://us.expasy.org/sprot>).

Real-time PCR. Real-time quantitative PCR was carried out using ABI Prism 7900HT Sequence Detection System and SYBR Green reagents from Applied Biosystems (Foster City, CA). Results of characterization studies confirmed the wide dynamic range and the reproducibility of this assay. Primers were designed using Primer Express v2.0 (Applied Biosystems) and listed in Table 1. The RT-PCR reaction mixture contained 1× SYBR Green PCR master mix, 0.25 U/μl Multiscribe reverse transcriptase, 0.4 U/μl RNase inhibitor, 400 nM forward and reverse primers, and 10 ng total RNA, in a volume of 10 μl. Each reaction was performed in triplicate in clear 384-well plates at 48°C, 30 min; 95°C, 10 min; then 95°C, 15 seconds, and 60°C, 1 min, for 40 cycles. This was followed by the construction of a dissociation curve through increasing the temperature from 60°C to 95°C at a ramp rate of 2%. A single predominant peak was observed in the dissociation curve of each gene, supporting the specificity of the RT-PCR product. Ct numbers (the number of cycles at which fluorescent signals reached a detection threshold that was set

within the exponential phase of PCR) were used to calculate the expression levels of genes of interest normalized to endogenous cellular 18S rRNA. The level of 18S rRNA was measured in parallel using primers (50 nM) from a ribosomal RNA control kit from Applied Biosystems.

Streptozotocin-induced diabetes in rats. Male Sprague-Dawley rats with a 250-300 g body weight were treated with an intraperitoneal injection of streptozotocin at 60 mg/kg body weight to induce type I diabetes. Streptozotocin was dissolved in 50 mM citrate buffer (pH 5.0) at 40 mg/ml. Rats were considered diabetic if their blood glucose (measured with a Glucometer) was higher than 250 mg/dl both 48 hours after the injection of streptozotocin and at the time of glomeruli isolation, i.e., one week after injection. The ratios between right kidney weight and body weight at the time of glomeruli isolation was 0.0047 ± 0.0002 (n=6) in streptozotocin-treated diabetic rats and 0.0037 ± 0.0001 (n=7) in control rats ($P < 0.05$).

Isolation of glomeruli. A commonly used sieving method (19), with some modifications, was used to isolate glomeruli from control and treated rats one week after the streptozotocin injection. Rats were anesthetized, and the left kidney flushed with ice-cold HBSS via the abdominal aorta. The renal cortex was cut into small pieces and transferred to a 50-ml beaker on ice. The tissue was ground up with a glass pestle and transferred to a stainless steel sieve with a pore size of 140- μ m. The sieve was rinsed with ~250 ml of ice-cold HBSS and the flow-through collected in a beaker on ice. The grinding and rinsing steps were repeated if large pieces of tissue remained on the sieve. The collected flow-through was poured onto another sieve with a pore size of 74- μ m. The sieve was rinsed extensively with ~500 ml of ice-cold HBSS. Glomeruli retained on the sieve were

collected and inspected under a microscope equipped with a cold dissecting station.

Glomeruli with >99% purity were pelleted by centrifugation and immediately re-suspended in 1 ml TRIzol reagent (Invitrogen) for RNA extraction.

Lipid peroxidation assay. Thiobarbituric acid reactive substance (TBARS) was measured as an index of lipid peroxidation. TBARS was measured as described previously (28, 29) with some modifications. Briefly, 100 μ l of cell homogenate was combined with 300 μ l of a 1:1:1 mixture of 15% TCA, 0.375% thiobarbituric acid, and 0.01% butylhydroxytoluene. After incubation at 95°C for 30 min, the reaction mixture was extracted with 1-butanol and the absorbance read at 535 nm. 1,1,3,3-methylmalonaldehyde was used as a standard.

Cellular reduced thiols assay. The amount of cellular reduced thiols was measured using Ellman reagent. 20 μ l of cell homogenate was combined with 75 μ l of reaction buffer (Tris-Cl 30 mM, pH 8.0, EDTA 3 mM), 25 μ l of Ellman reagent (1.19 mg/ml in methanol), and 400 μ l of methanol. The absorbance of the 3,000 \times g supernatant was read at 412 nm. N-acetyl-L-cysteine was used as a standard, and the amount of reduced thiols was normalized by protein content.

Statistics. Microarray data were analyzed as described above. For other data, Student t test or one-way ANOVA followed by Student-Newman-Keuls test was used when appropriate. $P < 0.05$ was considered significant. Results are shown as mean \pm SEM.

Results

1. Expression profiles

Five-day treatment of rat mesangial cells with high glucose (25 mM D-glucose) resulted in the up-regulation of 459 cDNA elements and the down-regulation of 151 compared to normal glucose controls, representing 3.5% of 17,664 cDNA elements examined. The description, GenBank Accession number, and mean and s.d. of the $\ln(\text{ratio})$ of each of the 610 differentially expressed cDNA elements are shown in Supplemental Table. The threshold t value was 2.0, and the false discovery rate was 4.3% (see Methods). A slightly smaller number of elements (568 elements) would be considered differentially expressed, while the false discovery rate would be reduced by more than one half to 1.9%, if an additional criterion of absolute $\ln(\text{ratio}) > 0.18$ (i.e., a change of more than 20%), was applied. This indicated that the majority of false positives were among the elements with smaller fold changes. We chose to report all identified elements without applying the additional $\ln(\text{ratio})$ criterion because of the potential functional importance of some expression changes that were small in magnitude.

A selected set of 145 differentially expressed cDNA elements is shown in Table 2 along with their GenBank Accession numbers, brief notes of additional functional information, Swiss-Prot IDs, and mean and s.d. of their $\ln(\text{ratio})$. These elements were emphasized because they represented genes that formed large clusters corresponding to several functional categories as shown in Table 2. Specifically, 21 elements were found to be involved in cell cycle and proliferation, 12 in the cytoskeleton, 15 in mitochondrial and energy metabolism, 5 in oxidative stress, 54 in protein synthesis, sorting, and degradation, 15 in signal transduction, and 24 in general transcriptional regulation. This

categorization was the result of bioinformatic analysis of all of the 610 identified elements (see Methods). An example of the analysis was the homology search for 263 EST elements that had not previously been found to be homologous with known genes. Homology with known genes (mostly rat or mouse genes) with a BLAST score of more than 200 was found for 65 of these 263 elements, expanding the list of elements that could be linked to some biological functions.

The expression profile of the 145 elements in Table 2 revealed several global characteristics of the effect of a 5-day exposure to high glucose on mesangial cells. First, high glucose appeared to induce an overall elevation of cellular activity and metabolism. This was supported by up-regulation of a large number of genes associated with cell cycle progression (e.g., cyclin B1, proliferating cell nuclear antigen, replication factor C), protein synthesis (e.g., eukaryotic initiation factor 4B, aspartyl-tRNA synthetase, eukaryotic initiation factor 5), and transcriptional activation (e.g., retinoic acid receptor RXR- α , general transcription factor II-1, cAMP-dependent transcription factor), and down-regulation of genes related to protein degradation (e.g., Protein-L-isoaspartate O-methyltransferase, cytosol aminopeptidase). The up-regulation of genes related to protein synthesis and the down-regulation of those for protein degradation were consistent with the known hypertrophic effect of high glucose on mesangial cells. Second, a smaller number of genes in several categories with apparently counteracting functions were also activated. Examples included genes involved in cell cycle arrest, such as cyclin G1 and prohibitin, and transcription repression, such as histone methyltransferase. Third, a somewhat surprisingly large number of genes related to protein sorting and trafficking

(e.g., RAB2, RAB7, vacuolar protein sorting 29, archain 1, ARL-6 interacting protein-1) were found to be differentially expressed.

116 differentially expressed elements shown in Supplemental Table, but not included in Table 2 because they did not seem to form large clusters of genes with similar roles, also had some known functions. Some of these genes were known to be important for the effect of high glucose on mesangial cells. Notable examples included two elements (GenBank Accession # AA964281 and AA964892), both encoding collagen type IV $\alpha 1$, that were both highly up-regulated. This is consistent with the known effect of high glucose to induce increases in extracellular matrix deposition. Furthermore, several genes identified and validated to be differentially expressed in previous screening studies (5, 17, 22, 35) were confirmed by the present study. These included thrombospondin 1 (5, 17), a gene related to extracellular matrix, and vitamin D3-upregulated protein, a gene emphasized by Kobayashi et al (22). However, many genes identified in previous screening studies were not confirmed by the present study, suggesting differences in species (human vs. rat) and treatment conditions (e.g., 21 days vs. 5 days) and possibly technique-related variations. Another well-known mediator in diabetic nephropathy, transforming growth factor- β (38, 48), was not represented in this array. When a gene was represented by more than one cDNA element on the array, changes in the same direction were usually observed in those elements. The magnitude of change, however, varied in some cases, which could result from subtle differences in the amount or sequence of the cDNA probes.

2. Thiol anti-oxidative pathway

Three cDNA elements representing glutathione peroxidase 1, peroxiredoxin 6, and thioredoxin 2 were found to be up-regulated by high glucose (see Table 2).

Glutathione peroxidase 1 is one of the major enzymes catalyzing the reduction of peroxides (such as hydrogen peroxide and lipid peroxide) using glutathione as the hydrogen donor (8). Peroxiredoxin 6 is a member of the peroxiredoxin family that has peroxide reducing activities similar to glutathione peroxidase 1 except that glutathione peroxidase 1 is selenium dependent, while peroxiredoxins are not (16, 43). Thioredoxin 2 is the mitochondria specific isoform of thioredoxin that plays an important role in the reduction of cellular peroxides and protein disulfide bonds (2, 14, 18).

The up-regulation of these 3 genes was of immediate interest to us because of the authors' long-time interests in oxidative stress (28, 34, 46). As shown in Figure 1, up-regulation of these genes would indicate an increase in the activity of the thiol anti-oxidative pathway. Since it was widely known that high glucose induces substantial increases in the level of reactive oxygen species in several cell types (3) including mesangial cells (20, 21), it appeared that the up-regulation of the thiol anti-oxidative pathway might be an adaptational response of mesangial cells that could buffer high glucose-induced oxidative stress. It is worth noting that other major anti-oxidative genes, such as Cu-Zn superoxide dismutase, Mn superoxide dismutase, thioredoxin, thioredoxin reductase, and catalase were not differentially expressed based on the microarray data.

To test this hypothesis, we first re-examined the mRNA levels of glutathione peroxidase 1, peroxiredoxin 6, and thioredoxin 2 using real-time PCR. As shown in Figure 2A, results of the real-time PCR analysis in the original as well as additional cell preparations validated the up-regulation of all 3 genes in rat mesangial cells in response

to high glucose. The absence of differential expression of thioredoxin and catalase was also validated by real-time PCR. High glucose similarly up-regulated the mRNA expression of glutathione peroxidase 1, peroxiredoxin 6, and thioredoxin 2 in human mesangial cells (Figure 2B), suggesting that this up-regulation was not likely the result of artificial culture conditions of one particular cell line. The expression of these genes in human proximal tubule epithelial cells, however, was not affected by high glucose, suggesting that this effect might be specific for certain cell types such as mesangial cells, rather than a non-specific cellular response.

mRNA expression levels of these genes were further examined in glomeruli of diabetic rats to determine whether the changes observed in cultured mesangial cells also occurred in vivo. Glutathione peroxidase 1 and thioredoxin 2 mRNAs were significantly up-regulated in glomeruli isolated from rats with one week of streptozotocin-induced diabetes compared to controls (Figure 2C). Peroxiredoxin 6, however, was not differentially expressed in glomeruli. Thioredoxin and catalase were not differentially expressed, either, similar to mesangial cells in culture.

We then examined the effect of high glucose on TBARS, an index of lipid peroxidation, and the amount of cellular reduced thiols in cultured mesangial cells. As shown in Figure 3, high glucose significantly increased TBARS in rat and human mesangial cells by 12% and 25%, respectively. Meanwhile, high glucose decreased the amount of cellular reduced thiols in rat and human mesangial cells by 13% and 21%, respectively. These changes support the presence of high glucose-induced oxidative injury and increases in the consumption of reduced thiols. On the other hand, the small magnitude of these changes suggested that either the effect of high glucose on lipid

peroxidation and thiol consumption was mild, or an otherwise larger effect was buffered by the activation of protective pathways. The latter possibility would be consistent with the up-regulation of thiol anti-oxidative gene expression shown above.

High glucose-induced oxidative stress would be exacerbated by suppression of the thiol anti-oxidative pathway if the up-regulation of this pathway had been buffering the oxidative damage. Indeed, thiol-oxidizing agents 5,5'-dithiobis(2-nitrobenzoate) (DTNB, 1 mM) or diamide (100 μ M) substantially exacerbated high glucose-induced increases of TBARS in rat mesangial cells by 3-5 fold (Figure 4A). DTNB or diamide alone did not have significant effects on TBARS when cells were cultured in media containing normal glucose supplemented with D-mannitol or L-glucose. DTNB similarly exacerbated high glucose-induced increase in TBARS in human mesangial cells (Figure 4B). Diamide at this dose, however, was cytotoxic to human mesangial cells, causing cell death regardless of glucose concentrations.

In summary, five days of high glucose exposure and one week of streptozotocin-induced diabetes up-regulated the mRNA expression of thiol anti-oxidative genes in mesangial cells in culture and glomeruli in vivo, respectively. High glucose slightly decreased the amount of cellular reduced thiols in mesangial cells, and high glucose-induced increases of lipid peroxidation were substantially exacerbated by thiol-oxidizing agents.

Discussion

The present study provided the first comprehensive profile of mRNA expression in rat mesangial cells cultured in normal and high glucose for 5 days. A hypothesis derived from the microarray data was tested, and for the first time the results demonstrated an adaptational role of the thiol anti-oxidative pathway in high glucose-induced mesangial cell abnormalities.

The expression profiles established in the present study exhibit several global characteristics that are consistent with pathological alterations known to occur in high glucose-treated mesangial cells or in diabetic glomeruli, such as accelerated proliferation (45), hypertrophy (42), and increased deposition of extracellular matrix (32). Perhaps more interestingly, a large number of genes in several categories whose importance in the effect of high glucose on mesangial cells had not been emphasized were found to be differentially expressed. One such category included at least 12 genes related to the cytoskeleton and cell-cell or cell-matrix interactions. The importance of the cytoskeleton in diabetic nephropathy has only been reported in a small number of studies (6, 47), including a previous screening using suppression subtractive hybridization (5). Another such category included a large number of genes related to protein sorting and trafficking (Table 2). The role these cellular components and activities play in the effect of high glucose on mesangial cells and in diabetic nephropathy deserves further study.

Another important global characteristic observed in the present study is that simultaneous activation frequently occurs for genes or pathways with apparently opposing functions (cell cycle progression vs. arrest, protein synthesis vs. degradation, transcriptional activation vs. repression, etc.). This constant balancing between acting and

counteracting cellular components could indeed be a general mechanism for achieving dynamic adaptation and precise control of cellular functions. Such a fundamental process is sometimes overlooked. One implication of this fundamental process is that obtaining a more reliable view of cellular functions may require evaluation of the balance among all redundant, complementary, and opposing pathways (27), rather than one or two isolated components or pathways.

Up-regulation of the thiol anti-oxidative pathway is an example of such dynamic adaptation. Increased generation of superoxide anion, possibly from the mitochondrial respiratory chain and other sources, has been proposed as a common event that activates various mechanisms contributing to the development of diabetic complications (3). Large increases of reactive oxygen species have been observed in endothelial cells (10, 36) and mesangial cells (20, 21) treated with high glucose as well as in glomeruli isolated from diabetic rats (23). Antioxidants and anti-oxidative genes such as superoxide dismutase have generally been shown to be beneficial in the treatment of diabetes and its complications, including diabetic nephropathy (7, 24, 25). The effect of high glucose and diabetes on anti-oxidative pathways per se, however, is more controversial. Various responses (up-regulation, down-regulation, or no changes) have been reported for several anti-oxidative genes (4, 15, 23, 37), which might be partially related to genetic susceptibility to diabetic complications. Results of the present study support the notions that the thiol anti-oxidative pathway in mesangial cells can be up-regulated by high glucose and diabetes and that such up-regulation may be an adaptational response that could partially buffer the deleterious effect of high glucose-induced oxidative stress.

Several important questions emerged from these data and could become interesting subjects for future studies. The *in vitro* and *in vivo* functional significance of high glucose-induced alterations in the expression of several pathways identified in the present study (in addition to the thiol pathway) obviously deserves investigation. It would also be worthwhile to profile gene expression in mesangial cells exposed to high glucose for a shorter or longer duration or in combination with other treatments. Expression profiling in tissues obtained directly from human subjects or animal models of diabetic nephropathy would be highly valuable (39, 44). In regard to the thiol pathway, it remains to be determined whether up-regulation of the thiol anti-oxidative pathway *in vivo*, as indicated by the data obtained from isolated glomeruli, is an intrinsic protective mechanism in diabetic nephropathy. If so, it would be important to determine whether this protective mechanism diminishes or becomes overwhelmed by injurious processes as the disease progresses and whether diabetic nephropathy can be ameliorated by maintaining or further enhancing this mechanism through gene delivery or other interventions.

Acknowledgement

The authors thank the technical staff for assistance in manufacturing microarrays and the Microarray Group in the Department of Physiology for helpful discussion. This study was supported in part by NIH grants HL-29587 and HL-49219.

Figure Legends

Figure 1. Alterations of the thiol anti-oxidative pathway by high glucose. Red font indicates genes up-regulated by high glucose (5 d) in rat and human mesangial cells. Black bold font indicates genes represented in the microarray, but not altered by high glucose. Gray font indicates genes not represented in the microarray. Genes encoding enzymes are shown in italics. ROOH, peroxides; GSH, reduced glutathione; Trx, thioredoxin; Trx2, thioredoxin 2; GPX1, glutathione peroxidase 1; PRDX6, peroxiredoxin 6; GSR, glutathione reductase; TXNR, thioredoxin reductase; TXNR2, thioredoxin reductase 2; GSSG, oxidized glutathione.

Figure 2. The up-regulation of thiol anti-oxidative genes was validated in rat and human mesangial cells as well as rat glomeruli by real-time PCR. The up-regulation of all three genes by high glucose (5 d) was statistically significant in both rat (*A*) and human (*B*) mesangial cells. GPX1 and TXN2, but not PRDX6, were also significantly up-regulated in glomeruli isolated from diabetic rats one week after streptozotocin injection (*C*). Gene expression levels in human mesangial cells and rat glomeruli were analyzed by real-time PCR. *, $P < 0.05$ vs. normal glucose treated cells or control rats. HG, high glucose; NG, normal glucose; GPX1, glutathione peroxidase 1; PRDX6, peroxiredoxin 6; TXN2, thioredoxin 2.

Figure 3. High glucose increased lipid peroxidation and decreased the amount of cellular reduced thiols slightly. Rat (*A*) and human (*B*) mesangial cells were treated

with high (HG) or normal (NG) glucose for 5 d. TBARS, thiobarbituric acid reactive substance. N=8~11. *, P<0.05 vs. normal glucose.

Figure 4. Thiol oxidizing agents exacerbated high glucose-induced lipid

peroxidation in mesangial cells. Rat (*A*) and human (*B*) mesangial cells were treated with high glucose (HG) in the absence or presence of 5,5'-dithiobis(2- nitrobenzoate) (DTNB, 1 mM) or diamide (100 μ M) for 5 d. As parallel controls, cells were treated with normal glucose in the absence or presence of DTNB or diamide at the same concentrations. Results were expressed as percent increases relative to corresponding normal glucose control with or without DTNB or diamide. Diamide at this dose was cytotoxic to human mesangial cells. TBARS, thiobarbituric acid reactive substance. N=6~11. *, P<0.05 vs. HG alone.

References

1. Adler S. Structure-function relationships associated with extracellular matrix alterations in diabetic glomerulopathy. *J Am Soc Nephrol.* 5(5): 1165-72, 1994.
2. Arner ES, Holmgren A. Physiological functions of thioredoxin and thioredoxin reductase. *Eur J Biochem.* 267(20): 6102-9, 2000.
3. Brownlee M. Biochemistry and molecular cell biology of diabetic complications. *Nature* 414: 813-818, 2001.
4. Ceriello A, Morocutti A, Mercuri F, Quagliaro L, Moro M, Damante G, Viberti GC. Defective intracellular antioxidant enzyme production in type 1 diabetic patients with nephropathy. *Diabetes.* 49(12): 2170-7, 2000.
5. Clarkson MR, Murphy M, Gupta S, Lambe T, Mackenzie HS, Godson C, Martin F, Brady HR. High glucose-altered gene expression in mesangial cells. Actin-regulatory protein gene expression is triggered by oxidative stress and cytoskeletal disassembly. *J Biol Chem.* 277(12): 9707-12, 2002.
6. Cortes P, Mendez M, Riser BL, Guerin CJ, Rodriguez-Barbero A, Hassett C, Yee J. F-actin fiber distribution in glomerular cells: structural and functional implications. *Kidney Int.* 58(6): 2452-61, 2000.
7. Craven PA, Melhem MF, Phillips SL, DeRubertis FR. Overexpression of Cu²⁺/Zn²⁺ superoxide dismutase protects against early diabetic glomerular injury in transgenic mice. *Diabetes.* 50(9): 2114-25, 2001.
8. Dickinson DA, Forman HJ. Glutathione in defense and signaling: lessons from a small thiol. *Ann N Y Acad Sci.* 973: 488-504, 2002.

9. Diehl F, Grahlmann S, Beier M, Hoheisel JD. Manufacturing DNA microarrays of high spot homogeneity and reduced background signal. *Nucleic Acids Res.* 29(7): e38, 2001.
10. Giardino I, Edelstein D, & Brownlee M. BCL-2 expression or antioxidants prevent hyperglycemia-induced formation of intracellular advanced glycation endproducts in bovine endothelial cells. *J. Clin. Invest.* 97: 1422-1428, 1996.
11. Haneda M, Koya D, Isono M, Kikkawa R. Overview of glucose signaling in mesangial cells in diabetic nephropathy. *J Am Soc Nephrol.* 14(5): 1374-82, 2003.
12. Hessner MJ, Wang X, Hulse K, Meyer L, Wu Y, Nye S, Guo SW, Ghosh S. Three color cDNA microarrays: quantitative assessment through the use of fluorescein-labeled probes. *Nucleic Acids Res.* 31(4): e14, 2003.
13. Hessner MJ, Wang X, Khan S, Meyer L, Schlicht M, Tackes J, Datta MW, Jacob HJ, Ghosh S. Use of a three-color cDNA microarray platform to measure and control support-bound probe for improved data quality and reproducibility. *Nucleic Acids Res.* 31(11): e60, 2003.
14. Hirota K, Nakamura H, Masutani H, Yodoi J. Thioredoxin superfamily and thioredoxin-inducing agents. *Ann N Y Acad Sci.* 957: 189-99, 2002.
15. Hodgkinson AD, Bartlett T, Oates PJ, Millward BA, Demaine AG. The response of antioxidant genes to hyperglycemia is abnormal in patients with type 1 diabetes and diabetic nephropathy. *Diabetes.* 52(3): 846-51, 2003.
16. Hofmann B, Hecht HJ, Flohe L. Peroxiredoxins. *Biol Chem.* 383(3-4): 347-64, 2002.

17. Holmes DI, Abdel Wahab N, Mason RM. Identification of glucose-regulated genes in human mesangial cells by mRNA differential display. *Biochem Biophys Res Commun.* 238(1): 179-84, 1997.
18. Holmgren A. Thioredoxin and glutaredoxin systems. *J Biol Chem.* 264(24): 13963-6, 1989.
19. Ito O, Alonso-Galicia M, Hopp KA, Roman RJ. Localization of cytochrome P-450 4A isoforms along the rat nephron. *Am J Physiol.* 274(2 Pt 2): F395-404, 1998.
20. Kang BP, Frencher S, Reddy V, Kessler A, Malhotra A, Meggs LG. High glucose promotes mesangial cell apoptosis by oxidant-dependent mechanism. *Am J Physiol Renal Physiol.* 284(3): F455-66, 2003.
21. Kiritoshi S, Nishikawa T, Sonoda K, Kukidome D, Senokuchi T, Matsuo T, Matsumura T, Tokunaga H, Brownlee M, Araki E. Reactive oxygen species from mitochondria induce cyclooxygenase-2 gene expression in human mesangial cells: potential role in diabetic nephropathy. *Diabetes.* 52(10): 2570-7, 2003.
22. Kobayashi T, Uehara S, Ikeda T, Itadani H, Kotani H. Vitamin D3 up-regulated protein-1 regulates collagen expression in mesangial cells. *Kidney Int.* 64(5): 1632-42, 2003.
23. Koya D, Hayashi K, Kitada M, Kashiwagi A, Kikkawa R, and Haneda M. Effects of Antioxidants in Diabetes-Induced Oxidative Stress in the Glomeruli of Diabetic Rats. *J Am Soc Nephrol* 14: S250-S253, 2003.
24. Kubisch HM, Wang J, Luche R, Carlson E, Bray TM, Epstein CJ, Phillips JP. Transgenic copper/zinc superoxide dismutase modulates susceptibility to type I diabetes. *Proc Natl Acad Sci U S A.* 91(21): 9956-9, 1994.

25. Kuroki T, Isshiki K, and King GL. Oxidative Stress: The Lead or Supporting Actor in the Pathogenesis of Diabetic Complications. *J Am Soc Nephrol* 14: S216-S220, 2003.
26. Liang M, Briggs AG, Rute E, Greene AS, Cowley AW Jr. Quantitative assessment of the importance of dye switching and biological replication in cDNA microarray studies. *Physiol Genomics*. 14(3): 199-207, 2003.
27. Liang M, Cowley AW Jr., Greene AS. High throughput gene expression profiling: A molecular approach to integrative physiology. *J Physiol*. 554(Pt 1): 22-30, 2004.
28. Liang M, Croatt AJ, Nath KA. Mechanisms underlying induction of heme oxygenase-1 by nitric oxide in renal tubular epithelial cells. *Am J Physiol Renal Physiol*. 279(4): F728-35, 2000.
29. Liang M, and Knox FG. Nitric oxide reduces the molecular activity of Na⁺,K⁺-ATPase in opossum kidney cells. *Kidney Int*. 56(2): 627-34, 1999.
30. Liang M, Yuan B, Rute E, Greene AS, Olivier M, Cowley AW Jr. Insights into Dahl salt-sensitive hypertension revealed by temporal patterns of renal medullary gene expression. *Physiol Genomics*. 12(3): 229-37, 2003.
31. Liang M, Yuan B, Rute E, Greene AS, Zou AP, Soares P, McQuestion GD, Slocum GR, Jacob HJ, Cowley AW Jr. Renal medullary genes in salt-sensitive hypertension: a chromosomal substitution and cDNA microarray study. *Physiol Genomics*. 8(2): 139-49, 2002.
32. Mason RM, Wahab NA. Extracellular matrix metabolism in diabetic nephropathy. *J Am Soc Nephrol*. 14(5): 1358-73, 2003.

33. Mauer SM, Lane P, Hattori M, Fioretto P, Steffes MW. Renal structure and function in insulin-dependent diabetes mellitus and type I membranoproliferative glomerulonephritis in humans. *J Am Soc Nephrol.* 2(10 Suppl): S181-4, 1992.
34. Morrison J, Liang M, and Cowley AW Jr. Renal expression of NAD(P)H oxidase and nitric oxide synthases in consomic rats: Using real-time PCR as a targeted profiling tool (abstract). *J Am Soc Nephrol* 14: 136A, 2003.
35. Murphy M, Godson C, Cannon S, Kato S, Mackenzie HS, Martin F, Brady HR. Suppression subtractive hybridization identifies high glucose levels as a stimulus for expression of connective tissue growth factor and other genes in human mesangial cells. *J Biol Chem.* 274(9): 5830-4, 1999.
36. Nishikawa T, Edelstein D, Du XL, Yamagishi S, Matsumura T, Kaneda Y, Yorek MA, Beebe D, Oates PJ, Hammes HP, Giardino I, Brownlee M. Normalizing mitochondrial superoxide production blocks three pathways of hyperglycaemic damage. *Nature.* 404(6779): 787-90, 2000.
37. Sechi LA, Ceriello A, Griffin CA, Catena C, Amstad P, Schambelan M, Bartoli E: Renal antioxidant enzyme mRNA levels are increased in rats with experimental diabetes mellitus. *Diabetologia* 40: 23–29, 1997.
38. Sharma K, Ziyadeh FN. Hyperglycemia and diabetic kidney disease. The case for transforming growth factor-beta as a key mediator. *Diabetes.* 44(10): 1139-46, 1995.
39. Susztak K, Sharma K, Schiffer M, McCue P, Ciccone E, Bottinger EP. Genomic strategies for diabetic nephropathy. *J Am Soc Nephrol.* 14(8 Suppl 3): S271-8, 2003.
40. Tusher VG, Tibshirani R, Chu G. Significance analysis of microarrays applied to the ionizing radiation response. *Proc Natl Acad Sci U S A.* 98(9): 5116-21, 2001.

41. United States Renal Data System. Accessed November 19, 2003 at <http://www.usrds.org/adr.htm>.
42. Wolf G, Ziyadeh FN. Molecular mechanisms of diabetic renal hypertrophy. *Kidney Int.* 56(2): 393-405, 1999.
43. Wood ZA, Schroder E, Robin Harris J, Poole LB. Structure, mechanism and regulation of peroxiredoxins. *Trends Biochem Sci.* 28(1): 32-40, 2003.
44. Yechoor VK, Patti ME, Saccone R, Kahn CR. Coordinated patterns of gene expression for substrate and energy metabolism in skeletal muscle of diabetic mice. *Proc Natl Acad Sci USA.* 99(16): 10587-92, 2002.
45. Young BA, Johnson RJ, Alpers CE, Eng E, Gordon K, Floege J, Couser WG, Seidel K. Cellular events in the evolution of experimental diabetic nephropathy. *Kidney Int.* 47(3): 935-44, 1995.
46. Yuan B, Liang M, Yang Z, Rute E, Taylor N, Olivier M, Cowley AW Jr. Gene expression reveals vulnerability to oxidative stress and interstitial fibrosis of renal outer medulla to nonhypertensive elevations of ANG II. *Am J Physiol Regul Integr Comp Physiol.* 284(5): R1219-30, 2003.
47. Zhou X, Hurst RD, Templeton D, Whiteside CI: High glucose alters actin assembly in glomerular mesangial and epithelial cells. *Lab Invest* 73: 372–383, 1995.
48. Ziyadeh FN, Sharma K, Ericksen M, Wolf G: Stimulation of collagen gene expression and protein synthesis in murine mesangial cells by high glucose is mediated by autocrine activation of transforming growth factor-beta. *J Clin Invest* 93: 536–542, 1994.

Table 1. Primer sequences for real-time PCR.

Gene	GenBank	Primer sequences	Amplicon
GPX1	X07365	Forward: TGAGAAGTGCGAGGTGAATGG	681-751
(rat)		Reverse: GTGCTGGCAAGGCATTCC	
PRDX6	NM_053576	Forward: GGCAAGAAATACCTCCGTTATACG	674-745
(rat)		Reverse: GCTGGTCGAGCAGTTGCA	
TXN2	U73525	Forward: AGCACGGGAAGGTGGTGAT	375-450
(rat)		Reverse: GCAGACACCTCGTACTCAATGG	
TXN	X14878	Forward: TCCAATGTGGTGTTCCTTGAAGTA	208-284
(rat)		Reverse: GGCATGCATTTGACTTCACAGT	
CAT	NM_012520	Forward: CCAGTACAACCTCCCAGAAGCCTAA	1577-1652
(rat)		Reverse: TCCCTTGGCAGCTATGTGAGA	
GPX1	Y00433	Forward: GAACGCCAAGAACGAAGAGATT	567-643
(human)		Reverse: GCATGAAGTTGGGCTCGAA	
PRDX6	BC035857	Forward: AGAGCTCCCATCTGGCAAGA	678-753
(human)		Reverse: CTCACAGCACCAACTTCTCCAA	
TXN2	NM_012473	Forward: CAGCCCACAGCGTTCCTAGT	868-943
(human)		Reverse: GGCACGAGGTTTCAGATTGG	

Abbreviations: GPX1, glutathione peroxidase 1; PRDX6, peroxiredoxin 6; TXN2, thioredoxin 6; TXN, thioredoxin; CAT, catalase.

Table 2. Large functional clusters of genes that exhibited differential expression in rat mesangial cells in response to high glucose^a.

Description	GenBank	Additional functional information	Swiss-Prot ^b	ln(ratio) ^c	s.d. ^d
Cell cycle and proliferation					
ESTs, similar to mouse tousled-like kinase 2	AA819648	chromatin assembly	Q86UE8	-0.29	0.13
ESTs, similar to mouse MOV-10 cyclin G-associated kinase	AI453858 AI071179	cell proliferation	P23249	-0.19	0.06 0.08
ESTs, similar to mouse proliferation-associated protein 2G4	AA955880		Q9UQ80	0.14	0.04
progesterone induced protein	AA955278	mRNA maturation; cell cycle	O95071	0.28	0.08
ESTs, similar to mouse Ran binding protein 1	AA957425	cell cycle, signaling	P34022	0.28	0.11
ESTs, similar to mouse dynactin 3	AA819405		Q9Z0Y1	0.34	0.05
splicing factor, arginine/serine-rich 5	AI028992	G1/S; mRNA splicing	Q09167	0.34	0.15
Prohibitin	AA866323	inhibit DNA synthesis	P24142	0.37	0.15
Cyclin G1	AA899938	G2/M arrest	P39950	0.42	0.18
Dihydrofolate reductase 1 (active)	AA900413	essential for DNA precursor synthesis	P00374	0.42	0.10
lamina associated polypeptide 2	AA925840	nuclear reassembly		0.42	0.13
ESTs, similar to human replication factor C 37 kDa subunit	AA819500	DNA replication	P35249	0.43	0.05
lamin A	AI070773		P48679	0.43	0.14
ESTs, similar to mouse paxillin-like protein (Hic5)	AA900090	TGFb1, H2O2-inducible, growth inhibition (senescence)	Q62219	0.45	0.11
Cyclin B1	AA998164		P30277	0.66	0.16
ESTs, similar to human histone H3.3	AA899072	nucleosome formation	P06351	0.77	0.12
Proliferating cell nuclear antigen	AA858643	DNA replication	P04961	0.80	0.17
Cyclin B1	AA998164	G2/M transition	P30277	0.82	0.19
cell division cycle 42 homolog (S. cerevisiae)	AA925473			0.84	0.21
ESTs, similar to mouse splicing factor, arginine/serine-rich 2	AA819369	cell cycle; mRNA splicing	Q62093	0.90	0.18
Cytoskeleton					
kinesin light chain 1	AA899876		P37285	0.28	0.08
afadin	AA819503	actin-binding, cell adhesion	O35889	0.31	0.07
ESTs, similar to mouse actin cross-linking family protein 7	AA858740			0.32	0.12
ESTs, similar to mouse alpha-parvin mRNA	AA964535	cell adhesion	Q9EPC1	0.34	0.09
ESTs, similar to mouse vinculin	AA900065	cell adhesion	Q64727	0.39	0.09

Rattus norvegicus mRNA for class I beta-tubulin, complete cds	AA819803			0.52	0.24
ESTs, similar to human microtubule-associated protein EB1	AA925661		Q15691	0.55	0.21
ESTs, similar to human ARP2/3 complex 21 kDa subunit	AA899189		O15145	0.66	0.31
ESTs, similar to mouse actin cross-linking family protein 7	AI072264		Q9UPN3	0.67	0.27
ESTs, similar to mouse ARP2 actin-related protein 2 homolog	AA875408		O15142	0.77	0.12
ESTs, similar to rat destrin	AI113089		P18282	0.89	0.18
alpha-tubulin	AI713807			1.26	0.24
Mitochondrial/energy metabolism					
Ketohexokinase	AI043767	ie, hepatic fructokinase: primary metabolism of dietary fructose	Q02974	-0.45	0.06
Hexokinase 1	AI535490	mitochondrial metabolism	P05708	-0.21	0.08
3-hydroxybutyrate dehydrogenase (heart, mitochondrial)	AA817846	mitochondrial metabolism	P29147	-0.18	0.08
ATP synthase, H ⁺ transporting, mitochondrial F1 complex, gamma polypeptide 1	AI044995	mitochondrial metabolism		0.14	0.06
ESTs, similar to rat succinate dehydrogenase cytochrome b560 subunit	AA817748	mitochondrial electron transport	Q9CZB0	0.23	0.08
branched chain keto acid dehydrogenase kinase	AA819287	mitochondrial aa catabolism	Q00972	0.41	0.17
brain acyl-CoA hydrolase	AA955288	fatty acid metabolism; transcription	Q64559	0.43	0.15
ESTs, similar to mouse NAD(P) transhydrogenase	AA874799	mitochondrial metabolism	Q61941	0.48	0.09
fatty acid synthase	AA875158	synthesis of long-chain fatty acids	P12785	0.50	0.16
solute carrier family 25 (mitochondrial carrier; dicarboxylate transporter), member 10	AA859666	mitochondrial transporter		0.52	0.19
ESTs, similar to rat protein phosphatase 1, regulatory subunit 3D	AI710557	glycogen metabolism	O95685	0.76	0.23
ATP citrate lyase	AA859689	acetyl-CoA and lipid synthesis	P16638	0.77	0.24
4-aminobutyrate aminotransferase	AA996705	mitochondrial function	P50554	1.13	0.24
Uncoupling protein 2, mitochondrial	AA998366	uncoupling oxidative Pi from ATP synthesis	P56500	1.21	0.39
Aldolase A, fructose-bisphosphate	AA924326	glycolysis	P05065	1.49	0.53
Oxidative stress					
Glutathione peroxidase 1	AA859104	thiol anti-oxidation	P04041	0.47	0.12
thioredoxin 2	AA817683	thiol anti-oxidation		0.51	0.19

ESTs, similar to rat glutathione alcohol dehydrogenase class III	AA998218		P12711	0.52	0.17
ESTs, similar to mouse oxidative stress protein A170	AI502045			0.71	0.21
peroxiredoxin 6	AA859664	thiol anti-oxidation	O35244	0.86	0.24
<i>Protein synthesis, sorting, and degradation</i>					
ribosomal protein S2	AA858970		P27952	-0.61	0.28
ESTs, similar to human splicing factor, arginine/serine-rich 8	AA996595	alternative splicing of fibronectin, etc	Q12872	-0.43	0.10
ESTs, similar to mouse synaptotagmin 4	AA819815	Ca ²⁺ -dependent vesicle trafficking or exocytosis	P40749	-0.41	0.18
ESTs, similar to mouse DEAD/H (Asp-Glu-Ala-Asp/His) box polypeptide 13 (RNA helicase A)	AI547754	RNA splicing		-0.40	0.12
Protein-L-isoaspartate (D-aspartate) O-methyltransferase	AA997617	protein repair or degradation	P22062	-0.36	0.10
ESTs, similar to human cytosol aminopeptidase	AA858780	protein processing and turnover	Q9CPY7	-0.29	0.08
ESTs, similar to rat serine protease MASP3	AA926053		Q8CIR7	-0.28	0.13
ESTs, similar to mouse CDC4 repeat unit-containing protein	AI071697	BLAST matches rat fwd2--protein degradation	Q9QUH1	-0.27	0.08
ESTs, similar to mouse splicing factor, arginine/serine-rich 7	AA957242		Q3R3E9	-0.26	0.12
ESTs, similar to mouse parkin mRNA	BF542359	ubiquitin-protein ligase	Q9WVS6	-0.25	0.10
ribosome associated membrane protein 4	AA818368		Q9R2C1	-0.21	0.04
ESTs, similar to rat ribosomal RNA	AA900647			-0.19	0.09
vesicle-associated membrane protein 5	AA924748	vesicle trafficking		0.17	0.07
palmitoyl-protein thioesterase	AA818995	lysosomal degradation	P45479	0.19	0.09
ESTs, similar to mouse mitochondrial 28S ribosomal protein S25	AA923855		Q9D125	0.23	0.10
eukaryotic initiation factor 5 (eIF-5)	AA997210	translation initiation	Q07205	0.24	0.11
ESTs, similar to yeast vacuolar protein sorting 26	AA924448		O75436	0.27	0.06
ESTs, similar to mouse eukaryotic translation initiation factor 2	AA819442	translation initiation	Q9Z0N1	0.27	0.11
ubc2e ubiquitin conjugating enzyme (E217kB)	AA955475	protein degradation	P70711	0.27	0.10
ESTs, similar to rat alpha-2-macroglobulin precursor	AA900290	trapping of major proteinase	P06238	0.28	0.09
ESTs, similar to human deoxyhypusine synthase	AA925151	initiation factor 5A modification	P49366	0.30	0.13
ESTs, similar to human WW domain binding protein 11	AA956713	nuclear protein binding	Q9Y2W2	0.32	0.10
unr protein	AA964605	RNA binding, translational initiation	P18395	0.33	0.01

ESTs, similar to human Golgi-specific brefeldin A-resistance guanine nucleotide exchange factor 1	AA924964	protein trafficking	Q92538	0.34	0.17
adaptor protein complex AP-1, beta 1 subunit	AA957995	protein sorting	P52303	0.35	0.17
ESTs, similar to mouse ubiquitin carboxyl-terminal hydrolase 23	AA963455	remove ubiquitin from protein--yielding a thiol		0.35	0.05
ERM-binding phosphoprotein	AA957976	cytoskeleton, protein trafficking	Q9JJ19	0.37	0.12
ESTs, similar to rat ubiquitin ligase Nedd4	AA957260	ubiquitin conjugation	Q62940	0.38	0.15
Protein-L-isoaspartate (D-aspartate) O-methyltransferase	AA901276	repair or degrade damaged proteins	P22062	0.39	0.16
eukaryotic initiation factor 5 (eIF-5)	AA923836	translation initiation	Q07205	0.40	0.10
aspartyl-tRNA synthetase	AA858763	translation	P15178	0.42	0.18
ESTs, similar to mouse splicing factor, arginine/serine-rich 1	AA819367		Q07955	0.44	0.11
ESTs, similar to human mRNA-associated protein mrnp 41	AI029703	mRNA transport and attachment	P78406	0.45	0.18
ESTs, similar to mouse RAB18, member RAS oncogene family	AA819494	endocytosis	P35293	0.46	0.22
ESTs, similar to mouse synaptosomal-associated protein	AA996892	vesicle trafficking		0.46	0.21
serine (or cysteine) proteinase inhibitor, clade B, member 5	AA875346	serpin family	Q8WW89	0.47	0.17
ESTs, similar to mouse protein translation factor SUI1	AA899335		P48024	0.48	0.23
RAB11a, member RAS oncogene family	AA963374	endosomal trafficking	P24410	0.49	0.18
Protein-L-isoaspartate (D-aspartate) O-methyltransferase	AA900410	repair or degrade damaged proteins	P22062	0.51	0.18
ESTs, similar to mouse ARL-6 interacting protein-1	AA900292	protein trafficking	Q9JKW0	0.51	0.25
ESTs, similar to mouse 26S proteasome-associated pad1 homolog	AI043800	proteasome		0.53	0.26
ESTs, similar to mouse archain 1, mRNA	AA963606	Golgi vesicle trafficking	Q8C0G7	0.53	0.19
ribosomal protein L14	AA874811		Q63507	0.54	0.11
ESTs, similar to mouse 26S proteasome regulatory subunit S3	AA964001	degradation of ubiquitinated proteins	O43242	0.56	0.27
ubiquitin-conjugating enzyme E2D 3 (homologous to yeast UBC4/5)	AA900426	protein degradation	P47986	0.59	0.20
ZAP 36/annexin IV	AI059765	exocytosis	P55260	0.63	0.23
ESTs	AA963305	proteasome		0.65	0.21
ESTs, similar to mouse vacuolar protein sorting 29	AA819445	protein sorting	Q9QZ88	0.67	0.17
staufer (Drosophila, RNA-binding protein)	AA956589	positioning mRNA and stimulating translation	O95793	0.73	0.16
RAB2, member RAS oncogene family	AA899406	protein sorting	P05712	0.88	0.32
RAB7, member RAS oncogene family	AA818669	protein transport	P09527	0.89	0.28

ESTs, similar to mouse eukaryotic translation initiation factor 4B	AA997766	translation initiation	P23588	0.92	0.12
ADP-ribosylation factor 4	AI454367	protein trafficking	P36403	1.56	0.27
polypyrimidine tract binding protein	AA900117	pre-mRNA splicing	Q00438	1.61	0.15
Signal transduction					
ESTs, similar to human cAMP-specific phosphodiesterase (PDE4D) mRNA	AI029492		Q08499	-0.45	0.08
ESTs, similar to mouse Tnf receptor-associated factor 3 (Traf3) gene	AA965179	TNF signaling	Q60803	-0.30	0.15
receptor-like tyrosine kinase	AI030581		Q9QW24	0.21	0.09
Guanine nucleotide-binding protein G-s, alpha subunit, Genbank no U51565	AA859005			0.29	0.11
ESTs, similar to mouse QKI protein	AA997832	RNA binding, nerve myelination, embryo survival	Q61110	0.32	0.15
ESTs, similar to mouse chimerin 2	AA866393	GTPase activating protein	Q03070	0.32	0.10
ESTs, similar to mouse SrcSH3 binding protein	AI059117		Q9QWY8	0.33	0.14
ESTs, similar to mouse diacylglycerol kinase, delta	AA963250		Q16760	0.34	0.16
2',3'- Cyclic nucleotide 3'-phosphodiesterase	AA963596			0.38	0.07
ESTs, similar to mouse hematopoietic cell specific Lyn substrate 1	AA925692	tyrosine kinase substrate	P49710	0.41	0.14
serine threonine kinase pim3	AA998554		O70444	0.42	0.11
ESTs, similar to mouse COP9 homolog, subunit 4	AA900596			0.59	0.26
serine/threonine protein kinase TAO2	AI716111		Q9JLS3	0.71	0.05
Zipper (leucine) protein kinase	AA874981	MAPKKK12	Q12852	0.73	0.16
PCTAIRE-1 protein kinase, alternatively spliced	AA956259	ser/thr kinase		1.00	0.21
Transcription					
nuclear transcription factor - Y beta	AA817843	transcription activator of collagen I, etc	P25208	-0.39	0.10
matrin 3	AI072656		P43244	-0.36	0.15
ESTs, similar to mouse Msx-interacting-zinc finger (Miz1)	AA819514	transcription factor interacting with Msx2	Q54987	-0.28	0.13
ESTs, similar to mouse transcription factor AP-2 gamma	AI045183		Q61312	-0.27	0.10
ESTs, similar to mouse heat shock factor 2	AA859671	transcription activator binding heat shock promoter	P38533	-0.26	0.10
ESTs, similar to mouse DNA-directed RNA polymerase I	AI059293	transcription of rRNA	P97304	-0.24	0.05
ESTs, similar to rat general transcription factor II I	AA819652			-0.23	0.10
ESTs, similar to mouse transcription factor Sp1	AA818466		O89090	-0.22	0.10

ESTs, similar to human mRNA for pur alpha	AI713633	transcription activator	Q00577	0.24	0.10
general transcription factor IIB	AA925106		P29053	0.26	0.09
NonO/p54nrb homolog	AA818542	transcription, mRNA splicing	O54725	0.28	0.08
ESTs, similar to human transcription factor IIE	AI059059			0.30	0.14
Cbp/p300-interacting transactivator, with Glu/Asp-rich carboxy-terminal domain, 2	AA963458		Q99967	0.30	0.13
ESTs, similar to mouse Suv39h histone methyltransferase	AA997899	transcriptional repression	O43463	0.31	0.11
CCCTC-binding factor (zinc finger protein)	AI030850	transcription repressor or activator	Q9R1D1	0.37	0.17
ESTs, similar to rat general transcription factor II I	AA900046	transcription repressor involved in cell cycle	Q9JI57	0.37	0.14
ESTs, similar to mouse MYC-associated zinc finger protein	AA997064	transcription activator	P56671	0.38	0.10
Aryl hydrocarbon receptor	AA859478	transcriptional factor	P41738	0.39	0.18
ESTs, similar to mouse cyclic-AMP-dependent transcription factor ATF-1	AA957629			0.43	0.18
ESTs, similar mouse to thyroid hormone receptor-associated protein	AA957565	transcription coactivation	O09000	0.47	0.23
ESTs, similar to mouse E2F transcription factor 4	AA819041	activation of cell cycle progression genes	Q16254	0.53	0.20
histone deacetylase 3	AI044356		O15379	0.56	0.11
ESTs, similar to mouse suppressor of variegation 3-9 homolog 1	AA963141	Histone methyltransferase, transcription repression	O54864	0.59	0.26
ESTs, similar to rat retinoic acid receptor RXR-alpha	AA925720	retinoic acid regulation of transcription	Q05343	0.86	0.40

^aSee Supplemental Table for a complete list of 610 differentially expressed elements.

^bMost Swiss-Prot numbers shown correspond to rat proteins. Mouse or human proteins are shown in some cases in order to provide indications for function.

^cLn(ratio) represents mean ln(ratio) of 4 separate array hybridizations between rat mesangial cells treated with high glucose and normal glucose (see Methods and Materials). Positive values indicate up-regulation by high glucose, while negative values indicate down-regulation.

^ds.d., standard deviation of ln(ratio)s from 4 array hybridizations.

Figure 1

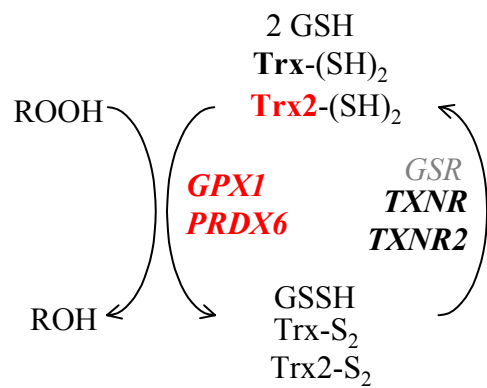


Figure 2

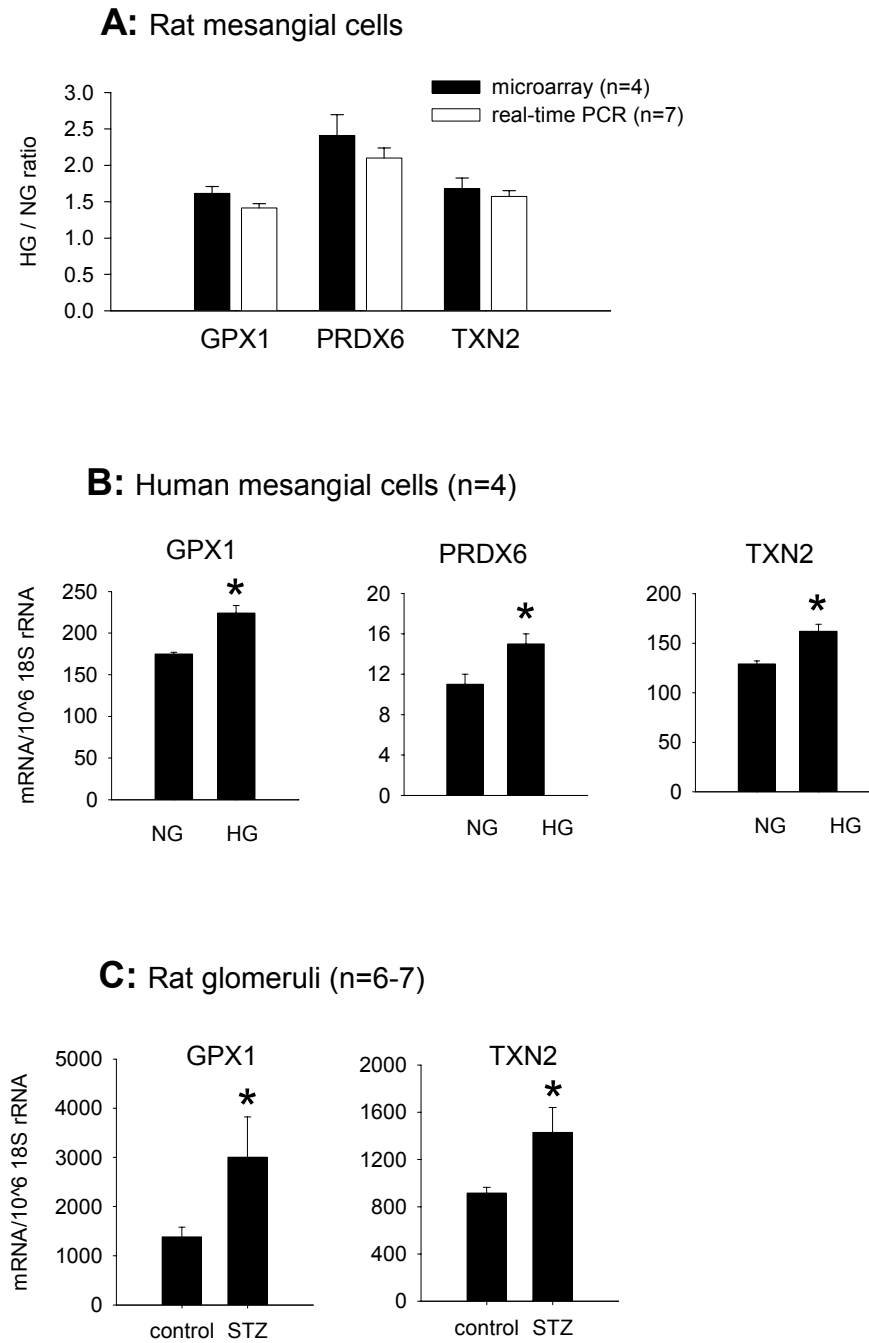


Figure 3

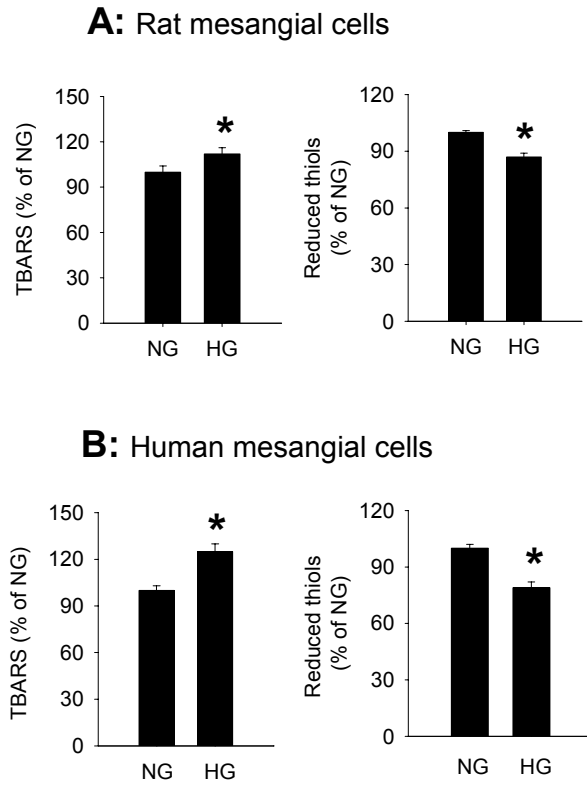


Figure 4

